THz wave in double-metal-film waveguides and the application of wavelength analysis

Jiamin Liu,[1,2,3] Huawei Liang,[2,3*] Min Zhang[2,3] and Hong Su[2,3]

[1]*College of Electronic Science and Technology, Shenzhen University, Shenzhen, 518060, China*

[2]*Shenzhen Key Laboratory of Laser Engineering, Shenzhen University, Shenzhen, 518060, China*

[3]*Key Laboratory of Advanced Optical Precision Manufacturing Technology of Guangdong Higher Education Institutes, Shenzhen University, Shenzhen, 518060, China*

**Corresponding author:* hwliang@szu.edu.cn

We propose the double-metal-film waveguides for THz wave guiding. The loss and field features are analyzed. In the application of wavelength analysis, we derive the formula of wavelength, and it can be used to analyze the wavelength of the THz sources according to mode field distribution in the dielectric-substrate slab. The penetrating capability of the THz wave is also discussed for different structure. When there is more energy in the dielectric-substrate slab, it will be better for wavelength analysis.

OCIS codes: *(260.3090) Infrared, far; (230.7370) Waveguides; (230.7390) Waveguides, planar.*

1. Introduction

In recent years, requirements of THz function devices [1-3] are frequently in the THz field, so the developments of these devices are essential. There have been all sorts of THz waveguides [4-6], such as metal wire waveguides [7-11], dielectric pipe waveguides [12-18], parallel plate waveguides [19-23], anti-resonant reflecting hollow waveguides [24,25], single metal plate waveguides [26-30], THz fibers [3,31,32], and metal tubes [33]. Since they are proposed, many aspects of new physics and applications have been researched, and many interesting theoretical and experimental conclusions have been given. These waveguides are used for different functions, such as endoscope [7] and sensor applications of metal wire [10, 11], dielectric pipe sensor [16,17], parallel plate sensor [22] and filter [23], single metal plate sensor [26-30], and THz switches [34,35]. These have promoted the THz field greatly. However, because the monochromaticity of THz sources [36] is a key factor, the achievement of single frequency transmission of THz beam is important. The function devices of monochromatic degree analysis of the THz sources are important and the development is essential. Meanwhile, like the metal films coated on the outside of double dielectric slabs [37,38], the waveguides have a feature like the parallel plate waveguides [19-23]. Although the craft is more difficult, the device can be lighter and easier to integrate. The effects of metal films coated on the inner side of the double dielectric slabs are not discussed yet and new application can be proposed.

In this paper, we study the features of the symmetrical dielectric-substrate double-metal-film waveguides theoretically. The application of wavelength analysis of THz sources is proposed, and the THz wave penetrating capability in the waveguide is analyzed in detail. The formula of wavelength has been derived, and we use this formula and the mode field distribution in the dielectric-substrate slab to analyze the wavelength of THz wave with different frequencies. The stronger penetrating capability will be better for applications of wavelength analysis. We believe that these results are meaningful in the design of THz function device.

2. The derive of dispersion equations of the double-metal-film waveguide

The TE mode of THz wave transmits in the double-metal-film waveguide (the structure is shown in Fig. 1) in z-direction, the air interval between the two metal films is $w = 2a$, thickness of each metal film is $t = b - a$, thickness of each dielectric-substrate slab is $d = c - b$.

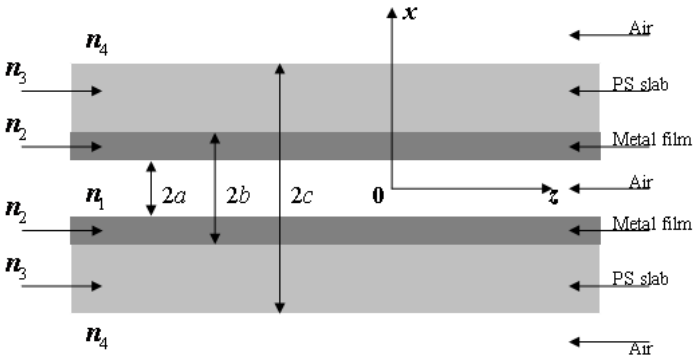

Fig. 1 The structure of the double-metal-film waveguide

In general, we suppose $n_4k_0 < n_3k_0 < \beta < n_2k_0 < n_1k_0$, $h_1 = (n_1^2k_0^2 - \beta^2)^{1/2}$, $h_2 = (n_2^2k_0^2 - \beta^2)^{1/2}$, $h_3 = (\beta^2 - n_3^2k_0^2)^{1/2}$, and $h_4 = (\beta^2 - n_4^2k_0^2)^{1/2}$, thus the even TE mode field components can be written as [25,37,39]:

$$E_y(x) = \begin{cases} A_{10}e^{-h_4(x-c)} & x \ge c \\ A_6e^{-h_3(x-b)} + A_7e^{h_3(x-b)} & b \le x \le c \\ A_2\cos h_2(x-a) + A_3\sin h_2(x-a) & a \le x \le b \\ A_1\cos(h_1x) & -a \le x \le a \\ A_4\cos h_2(x+a) + A_5\sin h_2(x+a) & -b \le x \le -a \\ A_8e^{-h_3(x+b)} + A_9e^{h_3(x+b)} & -c \le x \le -b \\ A_{10}e^{h_4(x+c)} & x \le -c \end{cases} \quad \textbf{(1)}$$

β is the complex propagation constant, and $k_0 = 2\pi/\lambda$ is the wave vector in vacuum. According to the boundary condition of the waveguide, the dispersion equation of TE mode is derived as [25,37,39]:

$$\tan(h_1a) = \frac{P_1 + P_2}{P_3 + P_4} \quad \textbf{(2)}$$

where $P_1 = [1 + \frac{h_2}{h_3}\tan h_2(b-a) - \frac{h_3}{h_4} - \frac{h_2}{h_4}\tan h_2(b-a)]e^{-h_3(c-b)}$,

$P_2 = [1 - \frac{h_2}{h_3}\tan h_2(b-a) + \frac{h_3}{h_4} - \frac{h_2}{h_4}\tan h_2(b-a)]e^{h_3(c-b)}$,

$P_3 = [-\frac{h_3}{h_4}\frac{h_1}{h_2}\tan h_2(b-a) + \frac{h_1}{h_4} + \frac{h_1}{h_2}\tan h_2(b-a) - \frac{h_1}{h_3}]e^{-h_3(c-b)}$, and

$P_4 = [\frac{h_3}{h_4}\frac{h_1}{h_2}\tan h_2(b-a) + \frac{h_1}{h_4} + \frac{h_1}{h_2}\tan h_2(b-a) + \frac{h_1}{h_3}]e^{h_3(c-b)}$.

Copper is adopted as the material of the metal film, and its relative permittivity $\varepsilon_2 = n_2^2$ can be gotten according to the Drude model [40].The material of dielectric slabs is Polystyrene (PS) with a refractive index of $n_3 = 1.58 - j0.0036$

[41]. The refractive index of air is $n_1 = n_4 = 1$.

3. Loss characteristics of the waveguide

When the air interval between the two metal films is w = 1 mm, the thickness of each metal film is t = 1 nm, and the thickness of each dielectric-substrate slab is d = 1 mm, we get the law of mode loss changing with the THz frequency by calculating Eq. (2), as shown in Fig. 2 (a) (solid line). We also get the group velocity of the corresponding frequency according to the equation $v_g = \dfrac{c}{n_{eff}\left(1+\dfrac{k_0}{n_{eff}}\dfrac{\mathrm{d}n_{eff}}{\mathrm{d}k_0}\right)}$, as shown in Fig. 2 (a) (dashed line). By Fig. 2(a), we can see there is a low cut-off frequency in the double-metal-film waveguide of TE mode, and the cutoff frequency of TE_1 mode can be obtained by the formula $f_c = \dfrac{c}{2w}$ [19]. In this case, f_c = 0.15 THz. Both the loss and dispersion has increased dramatically near the cut-off frequency. At 0.15 THz, the loss is 441.3 m^{-1}. The loss decreases with the increase of frequency, and at 2 THz, the loss is only 0.431 m^{-1}.

We also get the law of loss changing with the air interval w between two metal films at f = 1 THz, t = 1 nm, d = 1 mm, as shown in Fig. 2 (b). The figure shows when w is larger, the loss is very low (the loss is 0.188 m^{-1} at w = 2 mm), while the loss has increased dramatically in smaller w. At w = 0.15 mm, the loss is huge (2369.6 m^{-1}), because f = 1 THz has become the cutoff frequency of the waveguide. For w can be changed continuously, we can realize tunable high-pass filter by using this waveguide.

At f = 1 THz, w = 1 mm, d = 1 mm, the law of loss changing with each film thickness t is shown in Fig. 2 (c). We can see when the thickness of each film is thinner the loss is larger, such as at the thickness of the diameter of a copper atom t = 0.255 nm, the loss is 6.44 m^{-1}, while at t = 10 nm, the loss is only 0.15 m^{-1}. We also get the mode field in the metal film at t = 0.255 nm or 10 nm according to Eq. (1), as shown in Fig. 1 (d) and (e), respectively. We can see that when the films are thinner, the amplitude of the mode field in the metal film is larger (for example it is 0.0224 for t = 0.255 nm, while it is only about 0.00054 for t = 10nm), which causes the larger loss.

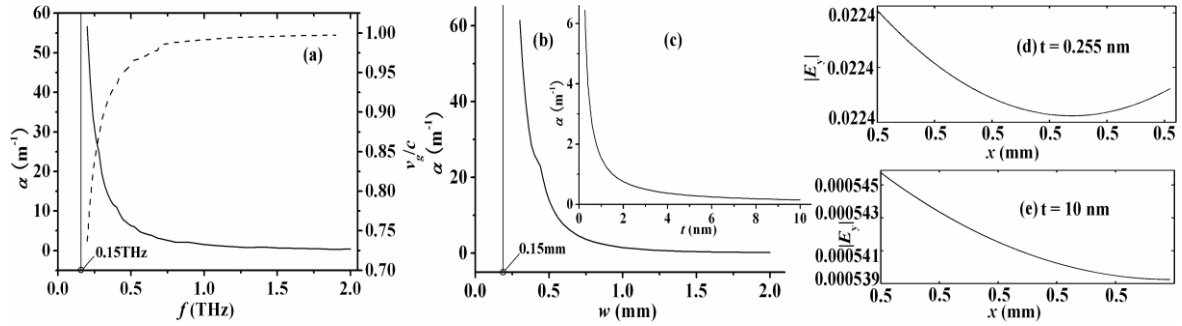

Fig.2 (a) The dependence of loss (solid line) on THz frequency f and the corresponding group velocity (dashed line), the perpendicular line is the location of the cut-off frequency. (b) The dependence of loss on air interval w between the two metal films, the perpendicular line is the location of the cut-off width of the air interval. (c) The dependence of loss on the thickness of each metal film t. (d) and (e) are mode field in metal films at f = 1 THz, w = 1 mm, d = 1 mm, t = 0.255 nm or 10 nm, respectively.

4. The application of wavelength analysis and the penetrating capability of THz wave in the waveguide

At w = 1 mm, t = 1 nm, d = 1 mm, we get the mode field distribution in the region of air interval and the dielectric-substrate slab when f = 0.2 THz, 0.5 THz and 1 THz, as shown in Fig. 3 (a) and (b) , respectively:

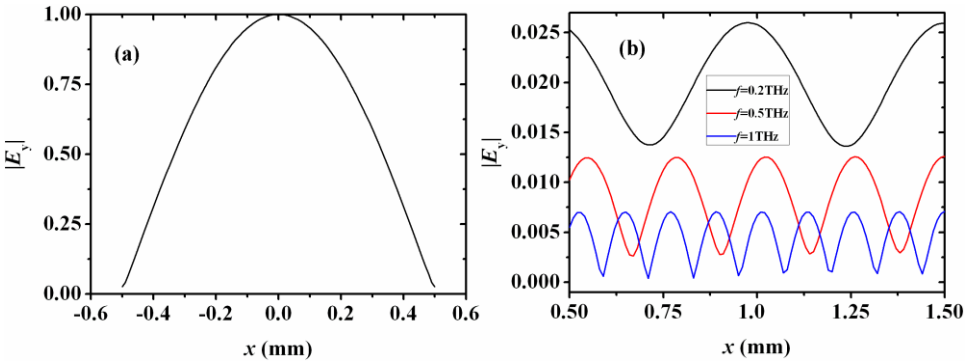

Fig.3 (a) The mode field distribution in the air interval. (b) The mode field distribution in the dielectric-substrate slab when f = 0.2THz (black line), 0.5THz (red line) and 1THz (blue line).

When the THz frequency changes, the mode field distribution of TE_1 mode in the air interval is basically unchanged, as shown in Fig. 3 (a). This is because even though the wavelength changes, most of the THz wave energy is confined in the middle air core of the waveguide for the reflecting on the double metal films. The even TE_1 mode has only one energy peak in the core. However, significant changes of the mode field distribution happen in the dielectric-substrate slab. By Fig. 3 (b), we can see that not only the amplitude of mode field within the dielectric-substrate slab changes significantly versus frequency, but also its total mode field phase and the initial phase on the interface between the dielectric-substrate slab and the metal film (left side) are significantly different. The oscillation distribution of the mode field in the slab is due to the limited thickness of the slab and the considerable energy in the slab. The penetrating capability of lower frequency is absolutely stronger. The initial phase of mode field on the interface between the dielectric-substrate slab and metal film moves to left with the increase of frequency, and the total mode field phases in the dielectric-substrate slab is also related to the wavelength of THz wave. By Fig. 3 (a), we can see the mode field is nadir on the interface of middle air and metal films, so according to Eq. (1), we can get:

$$\sqrt{n_1^2 k_0^2 - \beta^2}\, a = \frac{\pi}{2} \tag{3}$$

In the dielectric-substrate slab, the total phases of the mode field is $m\pi$, (m is a positive number), so we have:

$$\sqrt{n_3^2 k_0^2 - \beta^2}\, d = m\pi \tag{4}$$

According to Eq. (3) and (4), the wavelength of the THz wave can be gotten by the following relation:

$$\lambda = \sqrt{\frac{4(n_3^2 - n_1^2)}{\frac{m^2}{d^2} - \frac{1}{w^2}}} \tag{5}$$

According to Fig. 3 (b), a rough estimate of m at f = 0.2 THz, 0.5 THz, and 1 THz are $m \approx$ 1.9, 4.2, 8.2, respectively. We can get the wavelengths of THz wave: 1.51 mm, 0.60 mm and 0.30 mm, corresponding to f = 0.2 THz, 0.5 THz, and 1 THz, respectively by Eq. (5). The calculated wavelength is in good agreement with the theoretical value. In the case of unknown THz sources, even though the THz sources are not single frequency emitted, we can use this method to realize the analysis of wavelength and frequency spectrum.

When f = 0.5 THz, w = 1 mm, t = 1 nm, we get the rule of loss changing with the thickness d of each dielectric-substrate slab, as shown in Fig. 4 (a).

By Fig. 4(a), we can see the loss changes with d desultorily. This is mainly because different dielectric-substrate slab thicknesses will lead to the ruleless changing of initial phase in the dielectric-substrate slab, which makes the percentage of energy inside the metal films changes desultorily. The difference of dielectric-substrate slab thicknesses will affect the penetrating capability of the THz wave. The penetrating capability is stronger at the loss peak.

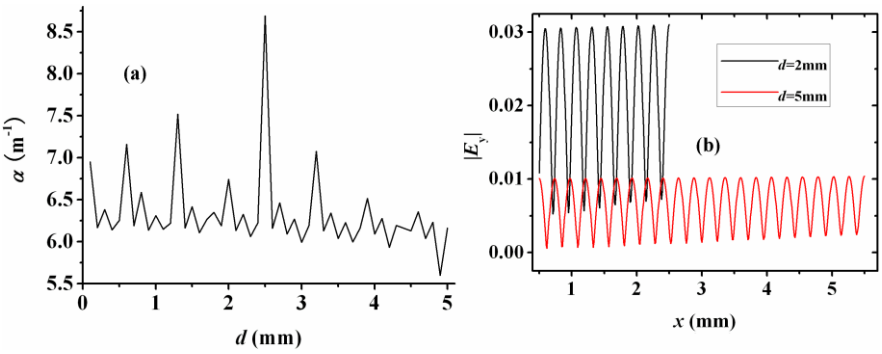

Fig.4 (a) The dependence of loss on the thickness d of each dielectric-substrate slab. (b) The mode field distribution of d = 2 mm (black line) and w = 5 mm (red line) in the dielectric-substrate slab.

We also get the mode field distribution in the dielectric-substrate slab at d = 2 mm (black line) and 5 mm (red line) as shown in Fig. 4 (b). By Fig. 4 (b), we can see the penetrating capability is absolutely stronger at d = 2 mm than at d = 5 mm. When the penetrating capability is stronger, the energy percentage in the metal films is also larger, which make the loss larger, such as the loss is 6.74 m^{-1} at d = 2 mm, while it is 6.16 m^{-1} at d = 5 mm. However, the loss of the waveguide is also related to the initial phase of mode field in the dielectric-substrate slab. We substitute the wavelength of 0.6 mm, w = 1 mm, and d = 2 mm or 5 mm, respectively into Eq. (5), and get the total phase number are m = 8.397 and 20.992, respectively. For the mode field on the interface of the dielectric-substrate slab and the outside air (right side) is always peak, the difference of the fractional portion of m tells us that the initial phase of mode field in the dielectric-substrate slab will be different. By Eq. (5), we can see the value of m is only related to d, when λ and w are confirmed. However, the relationship of the fractional portion of m on d is complex, which will lead to the initial phase changes in a complex rule, thus the loss change desultorily.

In order to know the relationship between penetrating capability and air interval w and the metal film thickness t, we get the mode field distribution in the dielectric-substrate slab at f = 0.8 THz, t = 0.255 nm, d = 1 mm and w = 0.5 mm, 2 mm or 4 mm, respectively, as shown in Fig. 5 (a):

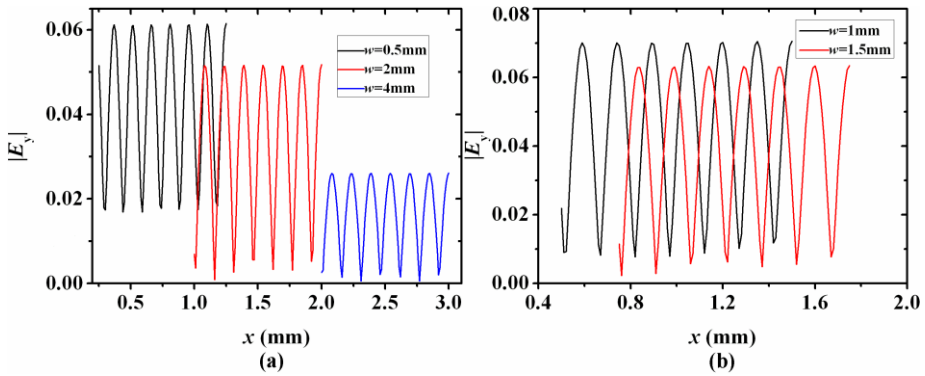

Fig.5 (a) The mode field distribution of w = 0.5 mm (black line), 2 mm (red line) and 4 mm (blue line) in each dielectric-substrate slab. (b) The mode field distribution of w = 1 mm (black line), 1.5 mm (red line).

Fig. 5 (a) shows that when w is smaller, the mode field amplitudes in the metal films are significantly larger (when w = 0.5 mm, the mode field amplitudes in the metal films is about 0.052; while it is only about 0.0070 w = 2 mm, and 0.0026 for w = 4 mm), this can be seen from that the initial phase in the slab moves to nadir gradually when w changes from 0.5 mm to 4 mm. So the loss is also larger for smaller w, (for example, $\alpha = 71.6\mathrm{m}^{-1}$ at w = 0.5 mm while it is only 0.0391 m^{-1} at w = 4 mm). We can also see that the nadir points of the field in the slab are lower when w is larger. However, the mode field amplitude in the slab has a largest value when w is between 0.5 mm and 2 mm. We also get the field in the slab when w = 1 mm and 1.5 mm, as shown in Fig. 5 (b), and find that the amplitude is about 0.07 at w = 1 mm, while it is about 0.06 both at w = 0.5 mm and 1.5 mm. However, the nadir points of w = 1.5 mm are lower. The energy contrast grade of the amplitude points to the nadir points is larger when w is between 1 mm and 1.5 mm, so it is better for wavelength analysis

in this range. It is worth to point out that when *w* is too small, the loss will be huge and the waveform will disappear, for the low frequency cut-off. Comparing Fig. 5 and Fig. 3 (b), 4 (b) we can see the penetrating capability is absolutely stronger when the film is thinner.

5. Conclusions

In conclusion, we study the features of the symmetrical dielectric-substrate double-metal-film waveguides theoretically. We propose the high-pass filter application of this waveguide using the tunable low cut-off frequency. We also propose the application of wavelength analysis of THz sources, and we have analyzed the penetrating capability of THz wave in the waveguide in detail. The formula of wavelength has been derived, and we analyze the wavelength of THz wave with different frequencies. The stronger penetrating capability will be better for applications of wavelength analysis, and we have discussed it for different *d*, *w* and *t*. We believe that these results are meaningful in the design of THz function device.

Acknowledgments

This work was supported in part by the National Natural Science Foundation of China under Grant 61405124, Natural Science Foundation of Guangdong Province, China under Grant 2014A030313560, the Specialized Research Fund for the Doctoral Program of Higher Education of China under Grant 20134408120002, and the Fund Project for Shenzhen Fundamental Research Programme under Grant JCYJ20130329140707824.

References

1. I. J. H. McCrindle, J. Grant, T. D. Drysdale, and D. R. S. Cumming, “Hybridization of optical plasmonics with terahertz metamaterials to create multi-spectral filters,” Opt. Express **21**(16), 19142-19152 (2013).
2. H. T. Chen, J. F. O’Hara, A. J. Taylor, R. D. Averitt, C. Highstrete, M. Lee, and W. J. Padilla, "Complementary planar terahertz metamaterials," Opt. Express **15**(3), 1084-1095 (2007).
3. H. Bao, K. Nielsen, H. K. Rasmussen, P. U. Jepsen, and O. Bang, “Design and optimization of mechanically downdoped terahertz fiber directional couplers” Opt. Express **22**(8), 9486-9497 (2014).
4. G. Gallot, S. P. Jamison, R.W. McGowan, and D. Grischkowsky, “Terahertz waveguides,” J. Opt. Soc. Am. B **17**, 851-863 (2000).
5. S. Atakaramians, S. Afshar V., T. M. Monro, and D. Abbott, “Terahertz dielectric waveguides” Advances in Optics and Photonics **5**, 169–215 (2013).
6. S. R. Andrews, “Microstructured terahertz waveguides” J. Phys. D: Appl. Phys. **47** 374004 (2014).
7. K.Wang, and D. M. Mittleman, “Metal wires for terahertz waveguiding”, Nature **432**, 376 (2004).
8. K. Wang, and D. M. Mittleman, “Dispersion of surface plasmon polaritons on metal wires in the terahertz frequency range”, Phys. Rev. Lett **96**, 157401 (2006).
9. T. Jeon, J. Zhang, and D. Grischkowsky, “THz Sommerfeld wave propagation on a single metal wire”, Appl. Phys. Lett **86**, 161904 (2005).
10. M. Wächter, M. Nagel, and H. Kurz, “Frequency-dependent characterization of THz Sommerfeld wave propagation on single-wires,” Opt. Express **13**(26), 10815–10822 (2005).
11. Nick C. J. van der Valka and Paul C. M. Planken, “Effect of a dielectric coating on terahertz surface plasmon polaritons on metal wires,” Appl. Phys. Lett. **87**, pp071106 (2005).
12. C.-H. Lai, Y.-C. Hsueh, H.-W. Chen, Y.-J. Huang, H.-C. Chang, and C.-K. Sun, “Low-index terahertz pipe waveguides,” Opt. Lett. **34**, 3457-3459 (2009).
13. C.-H. Lai, B. You, J.-Y. Lu, T.-A. Liu, J.-L. Peng, C.-K. Sun, and H. C. Chang, “Modal characteristics of antiresonant reflecting pipe waveguides for terahertz waveguiding,” Opt. Express **18**, 309-322(2010).
14. J.-T. Lu, Y.-C. Hsueh, Y.-R. Huang, Y.-J. Hwang, and C.-K. Sun, “Bending loss of terahertz pipe waveguides,” Opt. Express **18**, 26332–26338 (2010).
15. E. Nguema, D. Fèrachou, G. Humbert, J. L. Auguste, and J. M. Blondy, “Broadband terahertz transmission within the air channel of thin-wall pipe,” Opt. Lett. **36**, 1782–1784 (2011).

16. B. You, J.-Y. Lu, J.-H. Liou, C.-P. Yu, H.-Z. Chen, T.-A. Liu, and J.-L. Peng, "Subwavelength film sensing based on terahertz anti-resonant reflecting hollow waveguides," Opt. Express **18**(18), 19353–19360 (2010).
17. B. You, J.-Y. Lu, C.-P. Yu, T.-A. Liu, and J.-L. Peng, "Terahertz refractive index sensors using dielectric pipe waveguides," Opt. Express **20**(6), 5858–5866 (2012).
18. H. Bao, K. Nielsen, O. Bang, and P. U. Jepsen, "Dielectric tube waveguides with absorptive cladding for broadband, low-dispersion and low loss THz guiding", Scientific Reports **5**, 1-9 (2015).
19. R. Mendis and D. M. Mittleman, "An investigation of the lowest-order transverse-electric (TE_1) mode of the parallel-plate waveguide for THz pulse propagation," J. Opt. Soc. Am. B **26**, A6-A13 (2009).
20. R. Mendis and D. M. Mittleman, "Comparison of the lowest-order transverseelectric (TE_1) and transverse-magnetic (TEM) modes of the parallel-plate waveguide for terahertz pulse applications," Opt. Express **17**, 14839-14850 (2009).
21. J. Liu, H. Liang, M. Zhang, and H. Su, "Broadband terahertz transmission within the symmetrical plastic film coated parallel-plate waveguide" App. Opt. **53**(26), 6008-6012 (2014).
22. R. Mendis, V. Astley, J. Liu, and D. M. Mittleman, "Terahertz microfluidic sensor based on a parallel-plate waveguide resonant cavity," Appl. Phys. Lett. **95** (17), 171113 (2009).
23. R. Mendis, A. Nag, F. Chen, and D. M. Mittleman, "A tunable universal terahertz filter using artificial dielectrics based on parallel-plate waveguides," Appl. Phys. Lett. **97**(13), 131106 (2010).
24. J.-Y. Lu, H.-Z. Chen, C.-H. Lai, H.-C. Chang, B. You, T.-A. Liu, and J.-L. Peng, "Application of metal-clad antiresonant reflecting hollow waveguides to tunable terahertz notch filter," Opt. Express **19**(1), 162–167 (2011).
25. J. Liu, H. Liang, M. Zhang, and H. Su, "THz wave transmission within the metal-clad antiresonant reflecting hollow waveguides" Appl. Opt., **54**(14), 4549-4555 (2015).
26. M. Gong, T.-I. Jeon, and D. Grischkowsky, "THz surface wave collapse on coated metal surfaces" Opt. Express **17**(19), 17088-17101 (2009).
27. J. Saxler, J. G. Rivas, C. Janke, H. P. M. Pellemans, P. H. Bolı´var, and H. Kurz, "Time-domain measurements of surface plasmon polaritons in the terahertz frequency range" Phys. Rev. B **69**, 155427 (2004).
28. T. H. Isaac,W. L. Barnes, and E. Hendry, "Determining the terahertz optical properties of subwavelength films using semiconductor surface plasmons" Appl. Phys. Lett. **93**, 241115 (2008).
29. H. Liang, S. Ruan, S. Xu, M. Zhang, H. Su, and I. L. Li, "Modified surface plasmon polaritons with ultrahigh figures of merit on metal-gap–dielectric waveguides" Applied Physics Express **7**, 122001 (2014).
30. J. Liu, H. Liang, M. Zhang, and H. Su, "Metal plate for guiding terahertz surface plasmon-polaritons and its sensing applications" Opt. Communications **339** 222–227 (2014).
31. H. Bao, K. Nielsen, H. K. Rasmussen, P. U. Jepsen, and O. Bang, "Fabrication and characterization of porous-core honeycomb bandgap THz fibers" Opt. Express **20**(28), 29507-29517 (2012).
32. K. Nielsen, H. K. Rasmussen, A. J. L. Adam, P. C. M. Planken, Ole Bang, and P. U. Jepsen, "Bendable, low-loss Topas fibers for the terahertz frequency range" Opt. Express **17**(7), 8592-8601 (2009).
33. O. Mitrofanov1, and J. A. Harrington, "Dielectric-lined cylindrical metallic THz waveguides: mode structure and dispersion" Opt. Express **18**(3), 1898-1903 (2010).
34. H.-T. Chen, W. J. Padilla, J. M. O. Zide, S. R. Bank, A. C. Gossard, A. J. Taylor, and R. D. Averitt, "Ultrafast optical switching of terahertz metamaterials fabricated on ErAs/GaAs nanoisland superlattices," Opt. Lett. **32**(12), 1620–1622 (2007).
35. H. Zhang, P. Guo, P. Chen, S. Chang, and J. Yuan, "Liquid-crystal-filled photonic crystal for terahertz switch and filter," J. Opt. Soc. Am. B **26**(1), 101–106 (2009).
36. R A Lewis, "A review of terahertz sources" J. Phys. D: Appl. Phys. **47** 374001 (2014).
37. J. Liu, H. Liang, M. Zhang, and H. Su, "THz wave transmission within the metal film coated double-dielectric-slab waveguides and the tunable filter application" Opt. Communications, **351**, 103-108 (2015).

38. J. Liu, H. Liang, M. Zhang, and H. Su, “Coupling of Sommerfeld waves using odd TM mode of double-dielectric-slab waveguide,” J Opt 44(1), 53–58 (2014).
39. A. Yariv, Optical Electronics in Modern Communications (Oxford U. Press, Oxford, 2007).
40. M. A. Ordal, R. J. Bell, R. W. Alexander, Jr, L. L. Long, and M. R. Querry, “Optical properties of fourteen metals in the infrared and far infrared: Al, Co, Cu, Au, Fe, Pb, Mo, Ni, Pd,Pt, Ag, Ti, V, and W,” Appl. Opt. **24**(24), 4493–4499 (1985).
41. J. R. Birch, “The far-infrared optical constants of polypropylene, PTFE, and polystyrene,” Infrared Phys. **33**(1), 33–38, (1992).